
Effect of Blockage Shape on Unsteady Mixed Convective Nanofluid Flow Over Backward Facing Step

F. Fathinia^{1c} and Ahmed Kadhim Hussein²

¹ *Department of Thermofluids, Faculty of Mechanical Engineering
Universiti Teknologi Malaysia, MALAYSIA*

² *Mechanical Engineering Department, College of Engineering
Babylon University, IRAQ*

Abstract

The current work studies numerically the effects of four various types of blockage shapes on unsteady-mixed convection nanofluid flow over 2D horizontal backward facing step in a duct. SiO₂ is considered as nanoparticle with ethylene glycol (EG) as a base fluid, volume fraction of 2% and nanoparticle diameter of 20 nm to investigate the effect of blockage shape after analyzing the streamlines, velocity distribution, Nusselt number, and skin friction coefficient at different times. The downstream of the step was kept at temperature of 330 K, while other walls and sides of the duct were thermally insulated. The governing equations (continuity, momentum and energy) along with the boundary conditions are solved using the finite volume method (FVM). The Reynolds number was in the range of $50 \leq Re \leq 200$. The results reveal that after $\tau=5$ the trend of nanofluid flow and recirculation area near the step and behind the blockage shape doesn't change sensible and this time is selected as a quasi steady time and point of comparison. The velocity distributions in the front facing triangular blockage decrease and has the most value of skin friction coefficient after $Re=150$.

Keywords: Blockage shapes; Transient; Mixed convection; Backward facing step; Nanofluids.

1. Introduction

The geometry of backward facing step flow brings separation and further reattachment which exert a significant role in heat transfer processes. It has two aspects of valuable effect such as heat transfer improvement near the reattachment flow or a detrimental effect such as enhancement of dynamic structural load and drag. Energy system equipment, combustors, electronic cooling, cooling of turbine blades, cooling of nuclear reactors, environmental control systems, airfoils at the angle of attack, diffusers and many other devices are engineering applications of this geometry and occurs because of sudden expansion flow. Due to this notion, the problem of turbulent and laminar

^c Corresponding Author: F. Fathinia
Email: fa88fathinia@gmail.com

flows over backward facing step geometry in forced, mixed, and free convection has been discussed comprehensive, both numerically and experimentally [1, 2].

2. Previous work

Majority of currently research are focused on investigation of various steady flows over backward facing step by the incompressible flow. Al-aswadi et al. [1] studied laminar steady forced convection flow over a backward facing step placed in a 2D channel. They revealed that increasing the Reynolds number causes an increment in the reattachment length and the recirculation size. Kherbeet et al. [3] investigated numerically 2D laminar steady mixed convection flow over horizontal microscale backward facing step located in a duct. They found that the Nusselt number increases with increasing the Reynolds number and volume fraction. Lan et al. [4] conducted 3D simulations of turbulent steady flow over backward facing step in a rectangular duct. They concluded that the increase in the Reynolds number or aspect ratio eventuates in the lower average wall temperature and higher bulk Nusselt number.

Barrios-pina et al. [2] studied numerically mixed convection flow over a backward-facing step in a horizontal channel. They observed that the flow is steady in the primary recirculation area and it becomes periodic prior to chaos for high temperature difference.

Among literatures some of researchers have focused on installation of barrier or blockage shape in the way of flow. Cheng et al. [5] investigated the influence of the forced convection characteristics of backward facing step flow numerically in a 2D duct through the inserting of slotted and solid baffles onto the duct wall. They found that a slotted baffle can increase the average Nusselt number by the maximum 190%. Fathinia et al. [6] investigated 2D laminar mixed convection flow numerically over backward facing step with different inlet geometries in a channel. They revealed that Parallelogram inlet has the highest average velocity in all sections and highest average Nusselt number over downstream.

Kumar et al. [7] conducted numerically installation of circular cylinder as a blockage shape in a 2D duct in steady flow is effective for changing the velocity field of the backward-facing flow if the blockage situated at the suitable position. Nie et al. [8] demonstrated 3D forced convection steady flow over horizontal backward facing step in a channel to investigate the influence of using baffle on the heat transfer enhancement. They found that Installation of a baffle onto the upper wall enhances heat transfer and increases the magnitude of maximum Nusselt number at the stepped wall. Other researchers [3, 4, 9-21] have also focused on 2D and 3D forced and mixed convection flow over backward facing step. Their results revealed that near the side walls the reattachment area is larger compared to the center of the duct.

Nanofluids are one of the innovative ways to enhance the heat transfer for flows over backward facing step. Nanofluids are suspended particles such (Al_2O_3 , SiO_2 , TiO_2 , Ag, Au, etc) in conventional fluids such as (water, engine oil, etc). Several investigators have used different nanofluids with various base fluids to examine their effects on the heat transfer enhancement for flow over backward facing step. For instance, Murshed et al. [22], Timofeeva et al. [23], Zhang et al. [24], He et al. [25] have reported the influence of nanofluids on thermal conductivity enhancement and generally concluded that all nanofluids increased the thermal conductivity compared with their base fluids.

It is clear from the above literature review that the influence of blockage shapes on transient mixed convection nanofluid flow at backward facing step (BFS) in a duct seems not to have been investigated in the past and this has motivated the current study. In addition, the majority of the previous work on BFS has focused on using conventional fluids under steady state condition and there is very limited data reported in the open literature that included nanofluids over BFS. The present study analyzed 2D transient laminar mixed convection flow with the influence of using SiO₂ as a nanoparticles with ethylene glycol (EG) as a base fluid, 2% of nanoparticle volume fraction with 20 nm nanoparticle diameter, and different Reynolds number. The results of interests such as streamlines, velocity distribution, Nusselt number, and skin friction coefficient over the downstream wall of BFS are reported to demonstrate the influence of different blockage shapes on these parameters.

3. Numerical Model

3.1. Governing equations

The schematic of backward facing step (BFS) which has placed in a channel is shown in Figure 1. In mixed convection heat transfer, the wall down downstream of the step (X_e) is maintained at a uniform wall temperature of 330K and constant heat flux of 500W/m², while the straight wall that forms the other sides of the duct is thermally insulated and also the wall upstream of the step (X_i) and the backward facing step (S) are considered as adiabatic surfaces [3]. Several assumptions were made on the operating conditions of the BFS: (i) the BFS operates under unsteady state condition; (ii) the flow at the entrance is fully developed, incompressible and Newtonian; (iii) The straight wall, step wall and upstream wall were set to be thermally insulated; (iv) The external heat transfer effects and streamwise gradients of all quantities at the duct outlet were considered to be zero; (v) The ethylene glycol (EG) as a base fluid and SiO₂ as a nanoparticles is assumed to have a thermal equilibrium and no slip condition occurs.

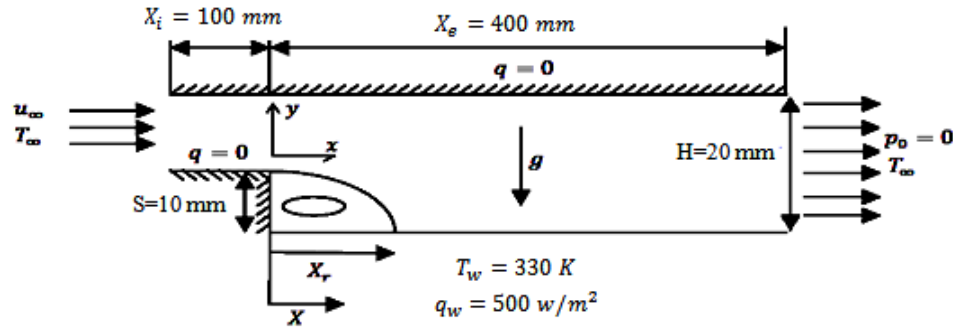


Figure 1. The schematic of backward facing step

Introducing the following dimensionless quantities:

$$U = \frac{u}{U_\infty}, V = \frac{v}{U_\infty}, X = \frac{x}{D_h}, Y = \frac{y}{D_h}, P = \frac{(p + \rho g x)}{\rho u_\infty^2}, \theta = \frac{(T - T_o)}{(q_w s / k)}$$

The governing equations for unsteady 2D flow are given as [26]:

$$\text{continuity: } \frac{\partial \rho}{\partial \tau} + \frac{\partial U}{\partial X} + \frac{\partial V}{\partial Y} = 0 \quad (1)$$

$$X, \text{Momentum: } \frac{DU}{D\tau} + \left(U \frac{\partial V}{\partial X} + V \frac{\partial U}{\partial Y} \right) = - \frac{1}{(1-\varphi) + \varphi \frac{\rho_s}{\rho_f}} \frac{\partial P}{\partial X} + \quad (2)$$

$$\frac{1}{\text{Re}_{((1-\varphi)^{2.5})} \left((1-\varphi) + \varphi \frac{\rho_s}{\rho_f} \right)} \left(\frac{\partial^2 U}{\partial X^2} + \frac{\partial^2 V}{\partial Y^2} \right) + \frac{Gr_x}{\text{Re}^2} \theta$$

$$Y, \text{Momentum: } \frac{DV}{D\tau} + \left(U \frac{\partial V}{\partial X} + V \frac{\partial U}{\partial Y} \right) = - \frac{1}{(1-\varphi) + \varphi \frac{\rho_s}{\rho_f}} \frac{\partial P}{\partial Y} + \quad (3)$$

$$\frac{1}{\text{Re}_{((1-\varphi)^{2.5})} \left((1-\varphi) + \varphi \frac{\rho_s}{\rho_f} \right)} \left(\frac{\partial^2 U}{\partial X^2} + \frac{\partial^2 V}{\partial Y^2} \right) + \frac{Gr_y}{\text{Re}^2} \theta$$

$$\text{Energy: } \rho \frac{DV}{D\tau} + U \frac{\partial \theta}{\partial X} + V \frac{\partial \theta}{\partial Y} = \frac{\partial Q}{\partial \tau} - \frac{1}{\text{Re Pr}} \left(\frac{\frac{k_{nf}}{k_f}}{(1-\varphi) + \varphi \frac{(\rho c_p)_s}{(\rho c_p)_f}} \right) \left(\frac{\partial^2 \theta}{\partial X^2} + \frac{\partial^2 \theta}{\partial Y^2} \right) \quad (4)$$

Where,

$$\text{Re} = \frac{\rho_f u_m D_h}{\mu_f}, \text{Pr} = \frac{\nu_f}{\alpha_f}, Gr_y = \frac{g \beta q_w s^4}{k \nu^2}, Gr_x = \frac{g \beta q_w s^4}{k u^2}$$

These governing equations along with the given boundary conditions are solved to obtain the velocity distribution, Nusselt number, and skin friction coefficient over downstream of BFS.

3.2. Grid sensitivity and model validation

3.2.1. Grid independence test

A grid independence test was done to evaluate the influences of grid sizes on the results. Four different computational grids were utilized, which are 140×40, 145×40, 150×30, and 160×30 with 1.01 in x-direction as a First Last ratio and 1.3 in y-direction as a successive ratio. All four grids are used to obtain the Nusselt number at the downstream wall by using air as a working fluid to choose the best grid size. Due to accuracy and computational time the grid of 160×30 was chosen to investigated the results.

3.2.2. Model validation

The code validation was performed on the basis of boundary conditions and geometry which were used by Kumar et al. [7]. Laminar forced convection flow was carried out over backward facing step in a 2D channel by presenting an adiabatic circular cylinder in the area of activity. The downstream bottom wall of channel was

kept by uniform temperature and other walls of backward facing step were maintained as adiabatic surfaces. The straight wall of the duct was kept at a constant temperature that is equal to the inlet fluid and velocity inlet was exposed in uniform. As can be seen in Figure 2, the present results are in good agreement with the results of Kumar et al. [7].

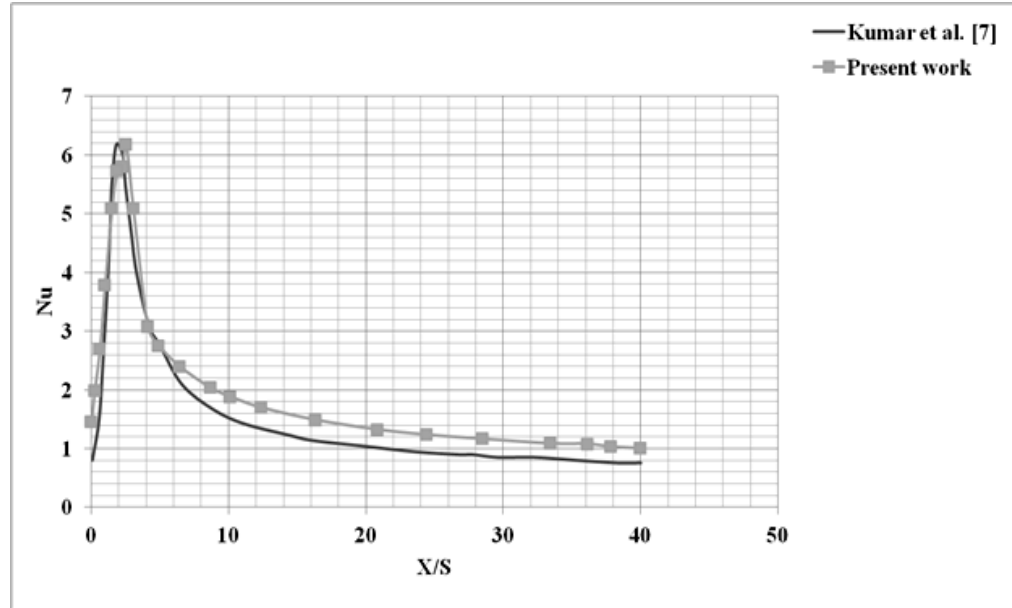


Figure 2. Comparison of the Influence of Reynolds number on the variation of the local Nusselt number distribution of the present work with the results of Kumar et al. [7]

3.3. Numerical procedure

The finite volume method was implemented by using FLUENT software version 6.2.3 to solve Eqs. (1) - (3). In this case, the numerical computations were investigated by solving the governing conservations along with the boundary conditions. The flow field was solved using the SIMPLE algorithm. The second-order upwind differencing scheme is considered for the convective terms. The diffusion term in the energy and momentum equations is approximated by the second-order central difference which gives a stable solution [27]. Quadrilateral elements and non-uniform grid system are exerted in the simulations. In order to increase the accuracy and decreasing the computational time, near to the step and close to the step corners are the places where the grid size is highly concentrated. The convergence criterion required that the maximum relative mass residual on the basis of the entrance mass be smaller than 1×10^{-3} .

3.4. Thermophysical properties of nanofluids

The thermophysical properties of nanofluids used in this study were obtained using the following equations:

$$\text{Density [28]: } \rho_{nf} = (1 - \phi)\rho_f + \phi\rho_s \quad (5)$$

$$\text{Heat capacity [28]: } (\rho C_p)_{nf} = (1 - \phi)(\rho C_p)_f + \phi(\rho C_p)_s \quad (6)$$

$$\text{Thermal expansion [27]: } (\rho\beta)_{nf} = (1 - \phi)(\rho\beta)_f + \phi(\rho\beta)_s \quad (7)$$

The β equations for different particle materials are shown in Table 1 as it is given by Vijjha and Das [29] and Vijjha et al. [30].

TABLE 1: β VALUES FOR DIFFERENT PARTICLES AND IT IS BOUNDARY CONDITIONS

Type of particle	β	Concentration (%)
SiO ₂	$1.9526(100\phi^{-1.4594})$ [24]	$1\% \leq \phi \leq 10\%$

$$\text{Effective thermal conductivity [28]: } k_{eff} = k_{static} + k_{Brownian} \quad (8)$$

Static thermal conductivity:

$$k_{static} = k_f \left[\frac{(k_{np} + 2k_f) - 2\phi(k_f - k_{np})}{(k_{np} + 2k_f) + \phi(k_f - k_{np})} \right] \quad (9)$$

Brownian thermal conductivity:

$$k_{brownian} = 5 \times 10^4 \beta \phi \rho_f C p_f \sqrt{\frac{KT}{2\rho_{np} R_{np}}} f(T, \phi) \quad (10)$$

Where the Boltzmann constant is: $k = 1.3807 \times 10^{-23} J / K$

Modelling function, $f(T, \phi)$ [30]:

$$f(T, \phi) = (2.8217 \times 10^{-2} \phi + 3.917 \times 10^{-3}) \left(\frac{T}{T_o} \right) \quad (11)$$

Dynamic viscosity [27]:

$$\mu_{eff} = \mu_f \times \frac{1}{\left(1 - 34.87 \left(\frac{d_p}{d_f} \right)^{-0.3} \times \phi^{1.03} \right)} \quad (12)$$

Equivalent diameter of base fluid molecule:

$$d_f = \left[\frac{6M}{N\pi\rho_{fo}} \right]^{\frac{1}{3}} \quad (13)$$

4. Results and discussion

The simulations are conducted for four various blockage shapes have been inserted in a fixed place of backward facing step channel. Figure 3 has shown these four blockage shapes with their exact location of inserting. In this case, SiO₂ has utilized as a nanoparticle with volume fraction of 2% and diameter of 20 nm with using ethylene glycol as a base fluid. The Reynolds number is in the range of $50 \leq Re \leq 200$ and the time scale is in the range of $0.1 \leq \tau \leq 10$. The effects of different blockage shapes and Reynolds number on the streamlines, velocity profile, Nusselt number, and skin friction coefficient for different times scale are interpreted and presented in this section.

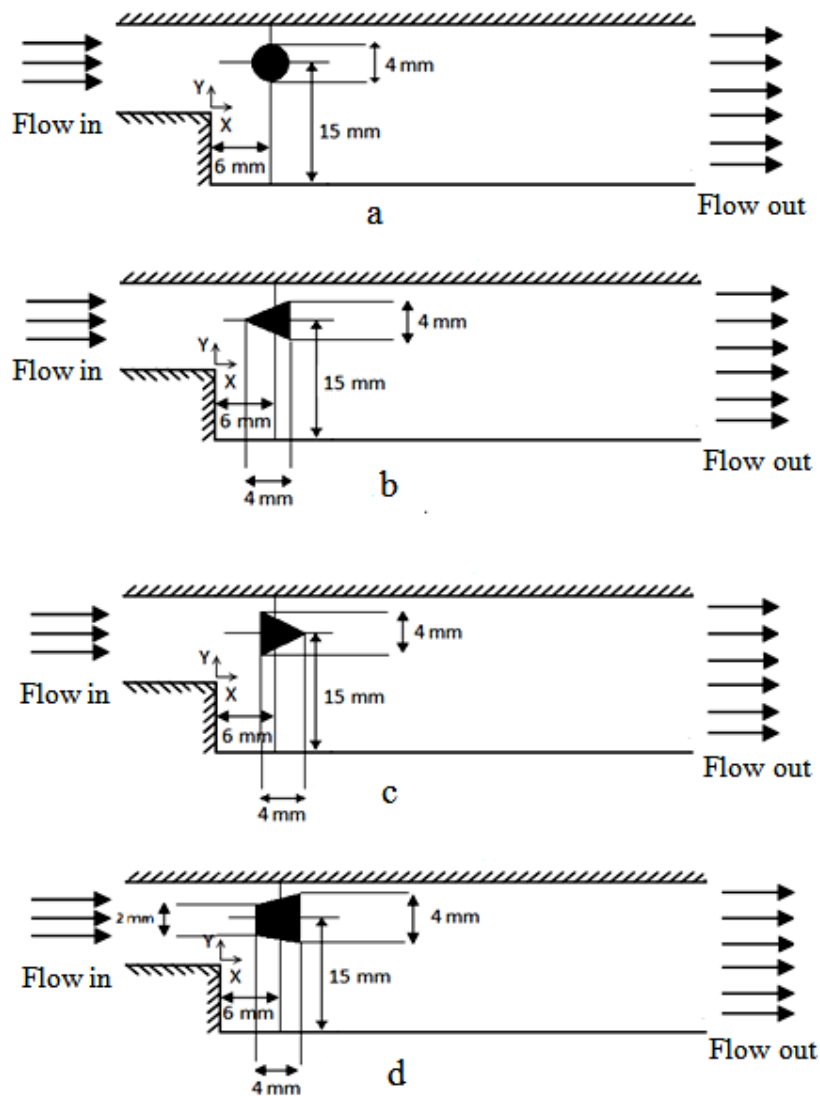


Figure3. The exact location of blockage shapes (a) Case 1: Circular blockage (b) Case 2: Back Facing Triangular blockage (c) Case 3: Front Facing Triangular blockage (d) Case 4: Trapezoidal blockage.

4.1. Flow pattern

The flow patterns of SiO_2 as a base fluid with 2% of volume fraction and 20 nm of diameter with ethylene glycol as a base fluid while pass from these four different blockage shapes across backward facing step channel are presented in Figures 4-7. For comparative research of influence of blockage shapes on streamlines in different times all the above cases (Figure 3) have been studied over the $\text{Re}=200$. A common note of Figures 4-7. is the swaying of major amount of nanofluid flow through the gap of between blockage shapes and top of step in backward facing step channel. In these figures the features of nanofluid flow in different times are clearly shown. As can be seen in Figures 4a, 5a, 6a and 7a, when the flow starts to move at $\tau=0.1$ there is not any particular noteworthy flow pattern. But when the time increase till $\tau=0.5$ the Figures 4b, 5b, 6b and 7b, present the creating of recirculation near the step and behind the blockage shapes. At this time, movement of nanofluid flow over and behind the blockage shapes is discovered to be influenced to some extent. $\tau=1$ is the next time scale and as can be clearly observed from Figures 4c, 5c, 6c and 7c, the

behavior of nanofluid flow is shown when coming from the upstream channel and obstructed by the blockage shapes and separated shear layer between the recirculation flow area and the primary flow. Quasi steady time is the moment in unsteady flow when after this time scale there is not any eminent changes. Due to finding the common quasi steady time for all of these cases, the time scale should be increased till discover this point. After analyzing, $\tau=5$ is selected as a quasi steady time and Figures 4d, 5d, 6d and 7d, have demonstrated the trend of nanofluid flow and primary recirculation area near the step. The stream lines in these figures are representing the nanofluid flow motion when passing over and beneath of baffles. The size of recirculation has increased maximally at this moment and there is not any significant alter after it. To ensure the accuracy of selected point as a quasi steady time, the time increased till $\tau=10$ to show that there is no different between the size of recirculation near the step and behind the blockage shape after $\tau=5$. So For comparative study Figures 4e, 5e, 6e and 7e, demonstrate that behind the blockage shape of case 3 (Front Facing Triangular blockage) the larger recirculation is created in aspect of size due to convergence form of triangular.

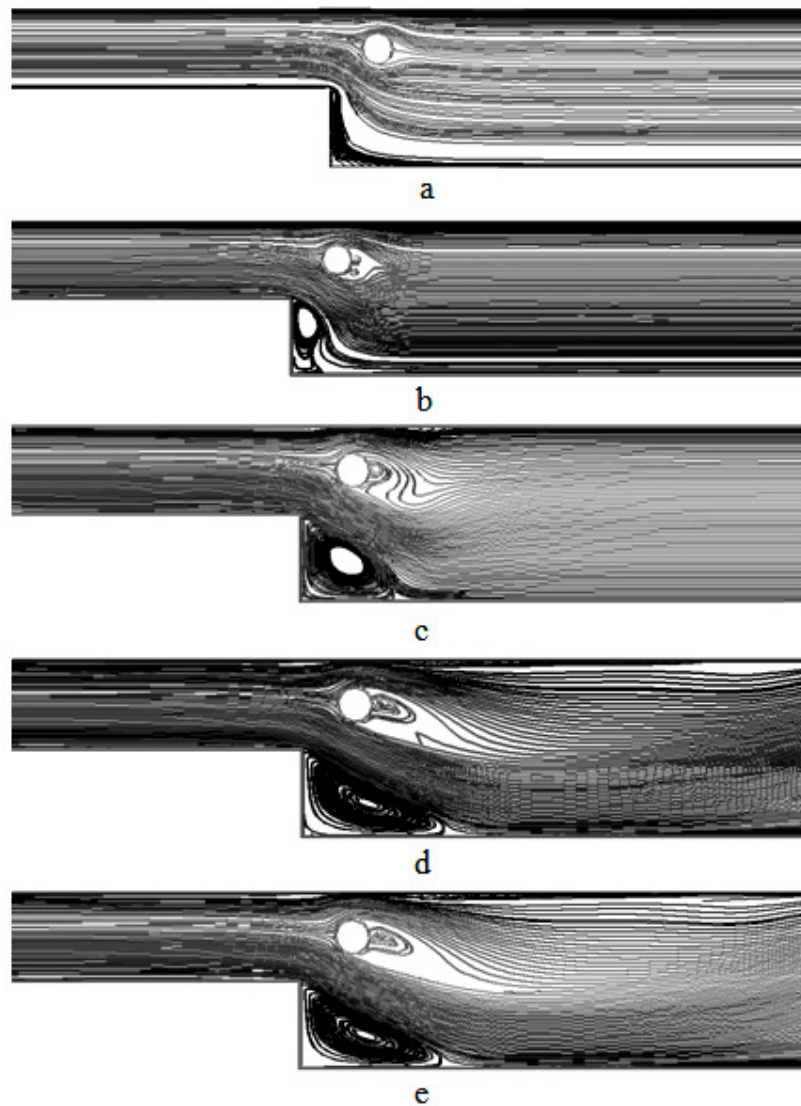


Figure 4. Streamline profiles of Case 1 (Circular blockage) for $Re=200$ at (a) $\tau=0.1$, (b) $\tau=0.5$, (c) $\tau=1$, (d) $\tau=5$ and (e) $\tau=10$

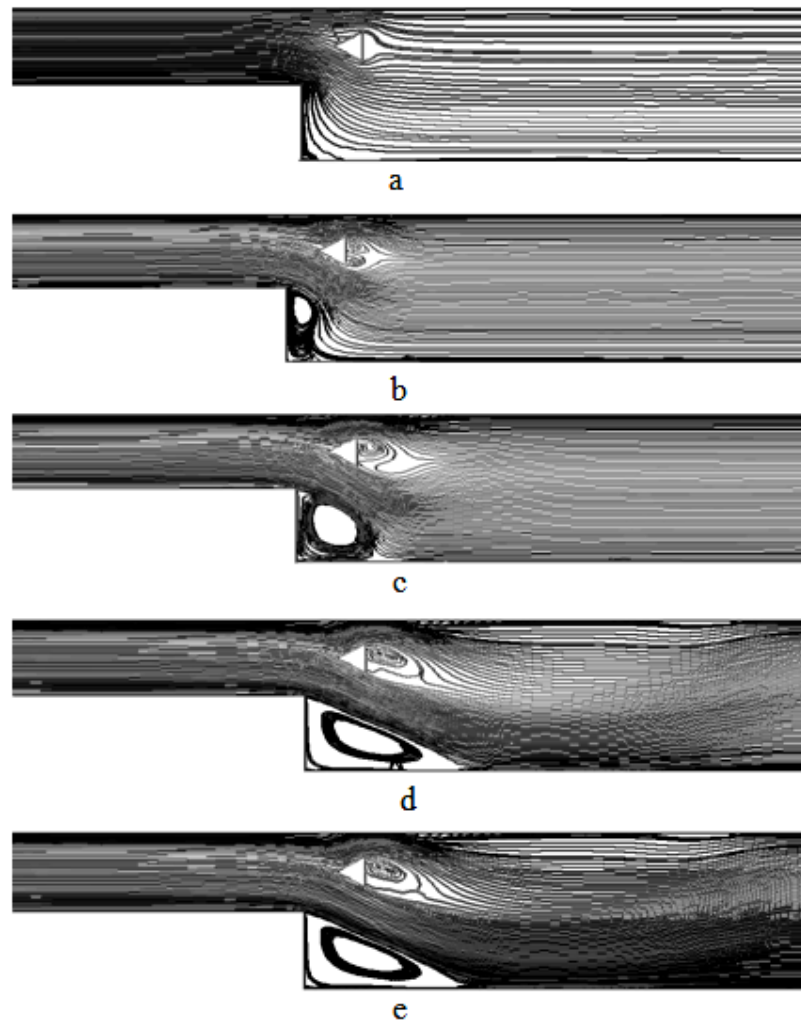


Figure 5. Streamline profiles of Case 2 (Back Facing Triangular blockage) for $Re=200$ at (a) $\tau=0.1$, (b) $\tau=0.5$, (c) $\tau=1$, (d) $\tau=5$ and (e) $\tau=10$

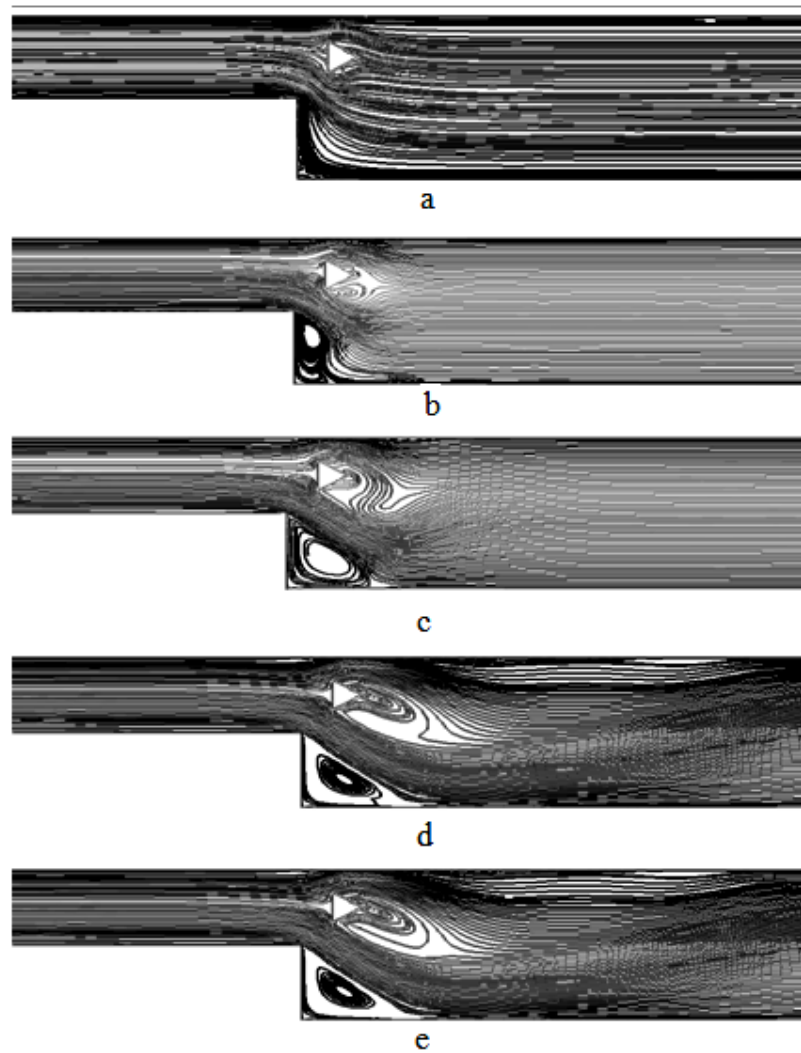


Figure 6. Streamline profiles of Case 3 (Front Facing Triangular blockage) for $Re=200$ at (a) $\tau=0.1$, (b) $\tau=0.5$, (c) $\tau=1$, (d) $\tau=5$ and (e) $\tau=10$

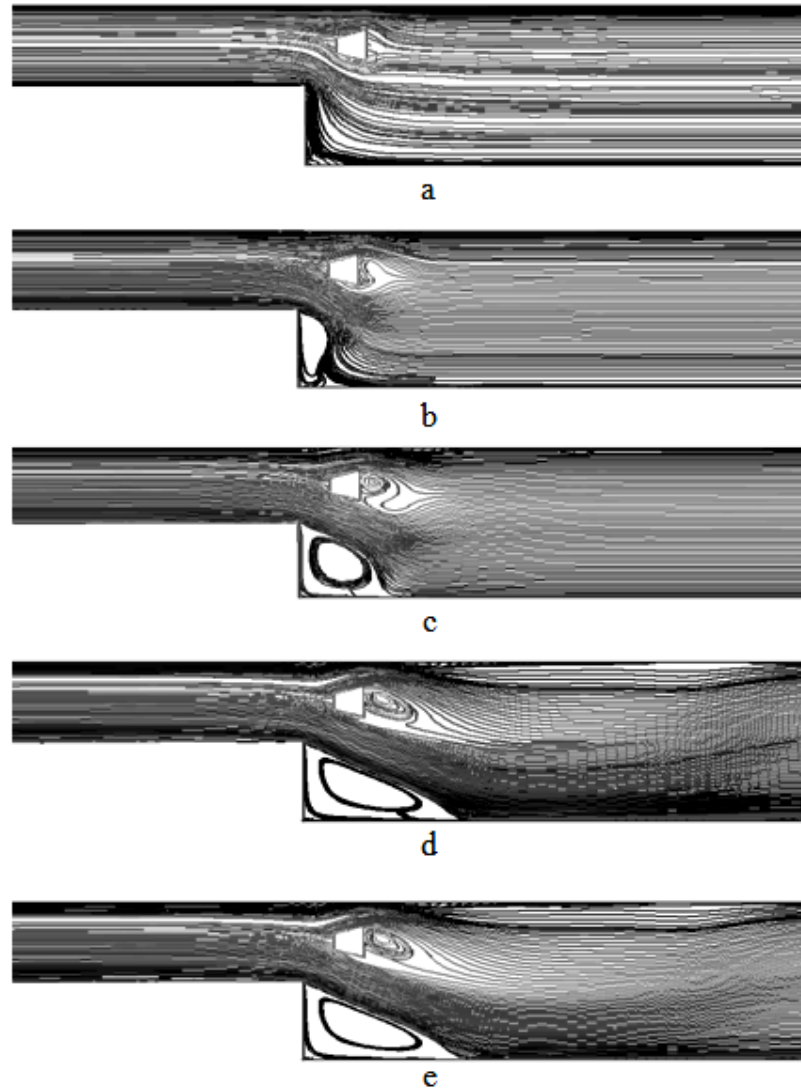


Figure 7. Streamline profiles of Case 4 (Trapezoidal blockage) for $Re=200$ at (a) $\tau=0.1$, (b) $\tau=0.5$, (c) $\tau=1$, (d) $\tau=5$ and (e) $\tau=10$

4.2. Velocity Profile

The influence of different blockage shapes on nanofluid flow field (SiO_2 -ethylene glycol) for 2% of volume fraction and 20 nm of nanoparticle diameter and $Re=200$ for four different times of $\tau=0.1$, $\tau=0.5$, $\tau=1$, and $\tau=5$ are shown in Figures 8-9. These figures are presented the velocity profile at $x/s=1$ along the downstream wall of backward facing step to show the velocity distribution over the duct. Figures 8a-c shows the velocity profile at $x/s=1$ for three different times of $\tau=0.1$, $\tau=0.5$ and $\tau=1$ before quasi steady point. It is clear that, the velocity profiles did not follow stable pattern and changed frequently at these times. The main note has been understood from these figures is by going up the time, the velocity distribution has found a regular pattern for study the effect of blockage shapes. For this purpose, Figure 9 has presented the velocity profile at quasi steady time ($\tau=5$). For all of these blockages can be seen two recirculation and it is obvious case 4 (Trapezoidal blockage) has a larger recirculation near the step while case 3 (Front Facing Triangular blockage) has a smallest. This phenomenon is created due to convergence style of case 4 and divergence style of case 3. Also case 3 causes to decrease the amount of velocity in

compared to other cases while case 4 improve the velocity and raising this value. In all cases the flow starts to redevelop and then approach the fully developed flow. Behind the blockage shapes of four cases can be observed recirculation but case 3 has the largest amount in compared the others because case 3 has the convergence style, conduct and focus the streamlines in one point. From the figures it is clear that the result of case 2 (Back Facing Triangular blockage) and case 4 (Trapezoidal blockage) due to divergence style are similar and has a bit difference and case 1 has a average result of these cases. This result occurs that the blockage shape with the form of case 4 can be used to increasing the value of velocity.

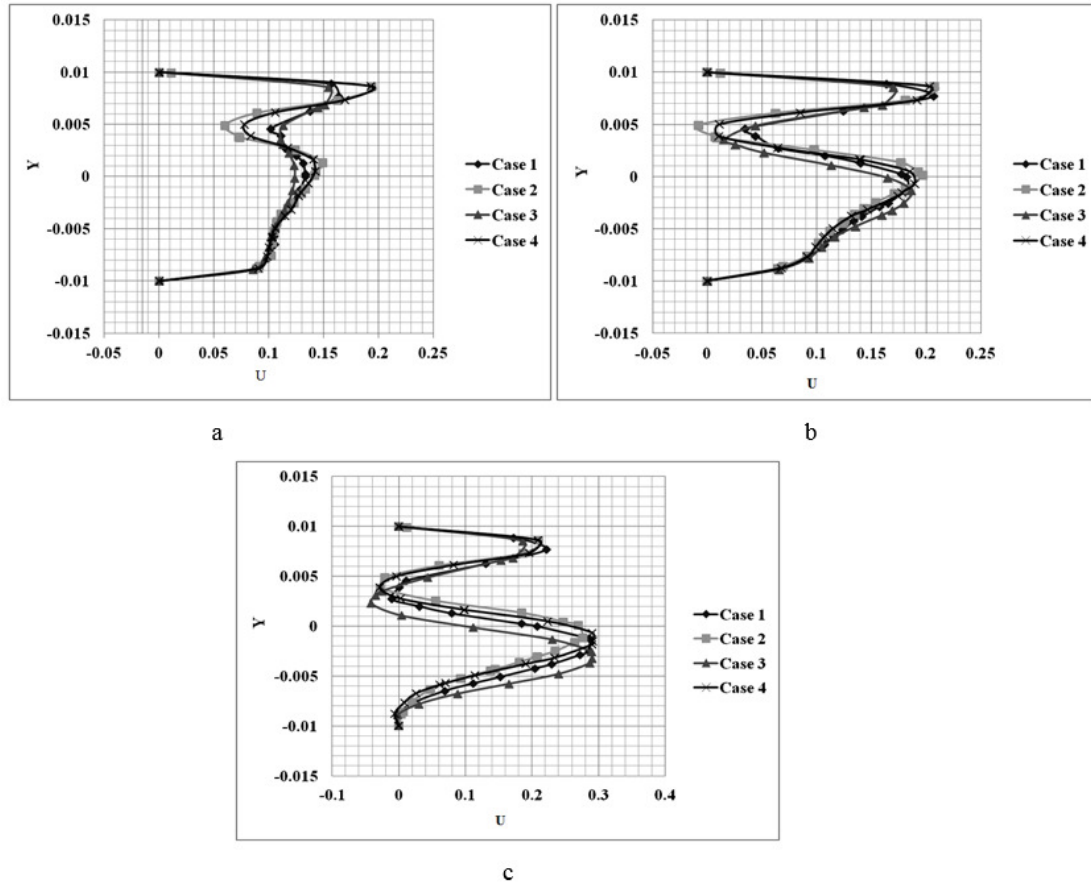


Figure 8. Velocity distributions of SiO₂-Ethylen glycol for Re=200 at x/s=1, and (a) $\tau=0.1$, (b) $\tau=0.5$ and (c) $\tau=1$

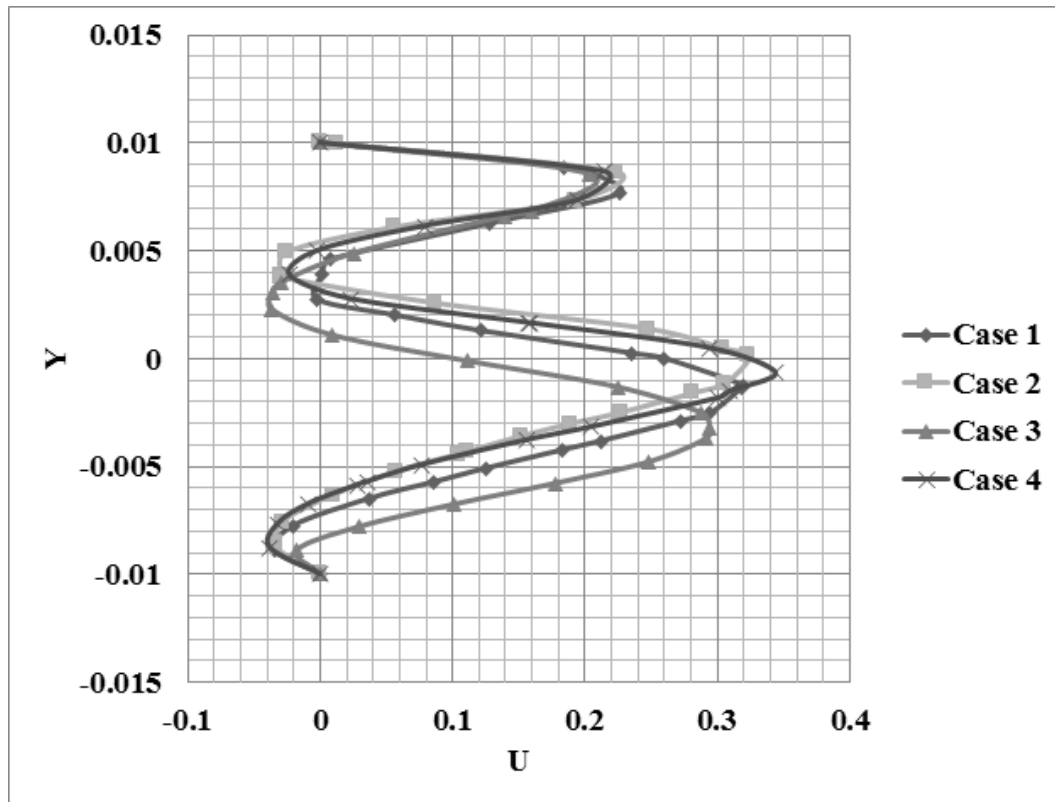


Figure 9. Velocity distributions of SiO₂-Ethylene glycol for Re=200 at x/s=1, and $\tau=5$ (quasi steady time)

4.3. Temperature fields

In this section, the velocity field is prepared at Re=200 while the constant temperature ($T_w = 330\text{k}$) with heat flux of 500 W/m^2 is considered over the downstream of backward facing step at $\tau=5$. As can be seen in Figure 10 under the effect of the reattaching flow, the temperature contours for the all cases tolerate local density around the flow-reattachment point. As a consequence, above the wall around the flow reattachment point a layer with rapid temperature gradient is created, which leads to heat transfer increment. Comparing all cases together, revealed that there is not any significant alteration except for the changing temperature in the proximity of step. This fact is clear by the similarity in temperature fields of case 1, 2, and 3 (Figures 10a, 10b, 10c). In case 4 (Figure 10d) tender temperature layers has been appeared over whole downstream of channel. Near to the reattachment point of the primary recirculation area and below the blockage shapes temperature fields for all cases display a marked compression and crowding of the temperature fields [7].

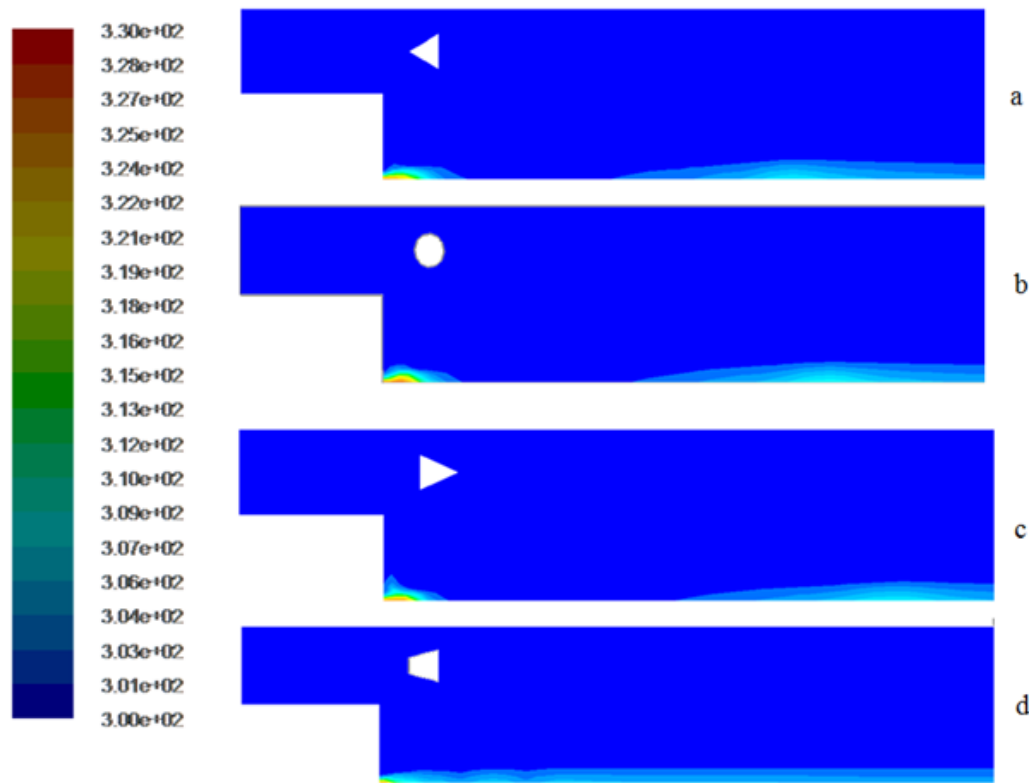


Figure 10. Temperature fields of SiO₂-Ethylene glycol for Re=200 at $\tau=10$ for (a) Case 1: Circular blockage (b) Case 2: Back Facing Triangular blockage (c) Case 3: Front Facing Triangular blockage (d) Case 4: Trapezoidal blockage

4.4. Nusselt number

The Nusselt number of various blockage shapes in a different Reynolds numbers at quasi steady time ($\tau=5$) is illustrated in this section. The Reynolds number has been considered is in the range of $50 \leq Re \leq 200$ and in each Reynolds number the average Nusselt number has been calculated and plotted in Figure 11. It is obvious the average Nusselt number of case 3 and case 4 has declined steadily by increasing Reynolds number while it can be generalized for case 1 and case 2 that at distances sufficiently away from the step (beyond the peak Nusselt number location) the average Nusselt numbers has risen gradually by going up the value of Reynolds number. On the other hand, the average Nusselt number of case 3 has the highest in each Reynolds number and case 4 has the lowest. Totally it can be concluded that case 2 will achieve a higher average Nusselt number by increasing Reynolds number after value of 200. In all cases it is obvious that the maximum peak of Nusselt number increases as Reynolds number increases due to proportion between the amount of convective heat transfer and velocity and the higher peak of Nusselt number corresponding to the reattachment point of the primary recirculation area.

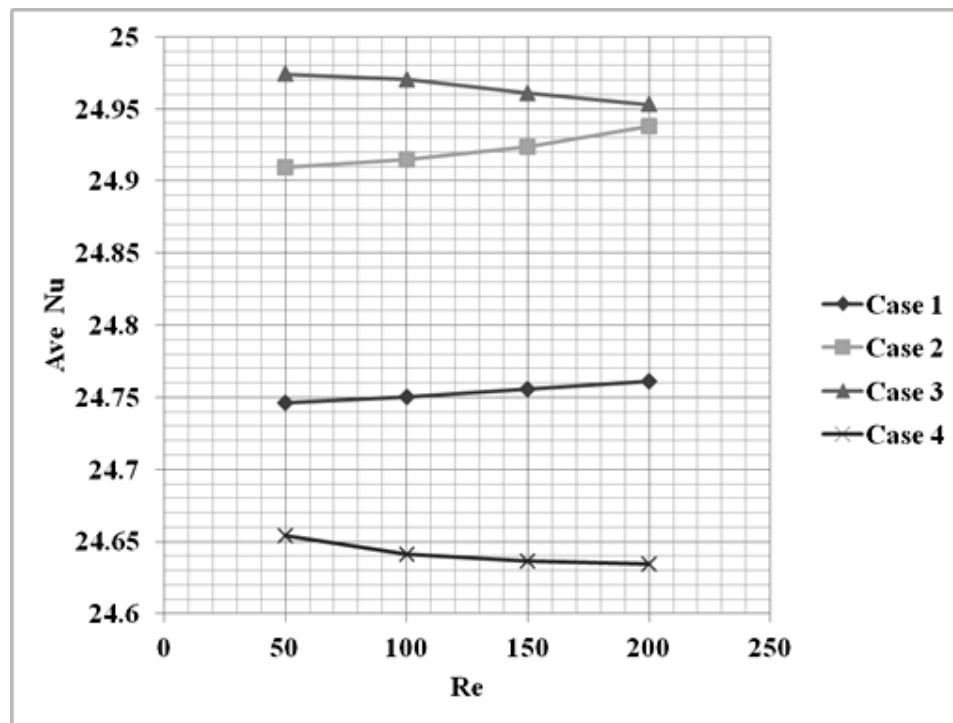


Figure 11. Average Nusselt number of SiO₂-Ethylen glycol for different Reynolds number at downstream for $\tau=5$ (quasi steady time)

4.5. Skin friction coefficient

The average value of skin friction coefficient of SiO₂-ethylene glycol with $\phi=2\%$, $d_p=20$ nm, and Reynolds number in the range of $50 \leq Re \leq 200$ on the downstream during various times between $\tau=0.1$ to $\tau=5$ is presented in this section. The effect of different blockage shapes on the skin friction coefficient is shown in Figure 12. It is clear that there is no influence of changing the blockage shape on the skin friction coefficient trend before $Re=150$ and all the cases have the same skin friction coefficient value. From the figure, the differences will be appeared by increasing the value of Reynolds number. As can be seen, case 3 has the most value of skin friction coefficient after $Re=150$ due to this fact that the skin friction coefficient is inversely proportional to the velocity and case 3 cause to reduce the velocity and had a less value of it in comparison the other shapes. It is observed that both the wall shear stress and skin friction coefficient have the same trend but with different values. They are not presented in this paper due to the space limitation.

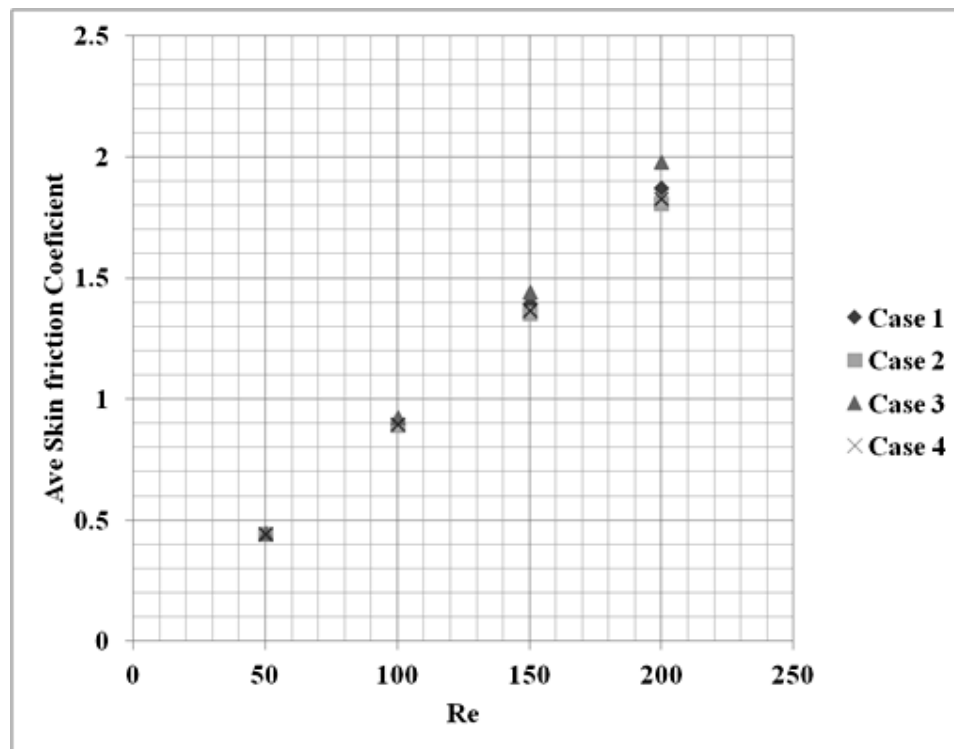


Figure 12. Average Skin friction coefficient of SiO₂-Ethylen glycol for different Reynolds number at downstream for $\tau=5$ (quasi steady time)

5. Conclusions

Numerical simulations for 2D transient mixed convection of four different blockage shapes with SiO₂ as a nanoparticles and ethylene glycol as a base fluid were discussed. Finite volume method was used to solve the governing equations with certain assumptions and appropriate boundary conditions for the present study. Results revealed that after $\tau=5$ the trend of nanofluid flow and recirculation area near the step and behind the blockage shape didn't change sensible and this time was selected as a quasi steady time and point of comparison. The velocity distributions in the case 3 decrease due to divergence style and has the most value of skin friction coefficient after $Re=150$ due to this fact that the skin friction coefficient is inversely proportional to the velocity. Furthermore, the average Nusselt number of case 3 has the highest in each Reynolds number and case 4 has the lowest.

References

- [1] Al-Aswadi, A., H. Mohammed, N. Shuaib and A. Campo, *Laminar forced convection flow over a backward facing step using nanofluids*. International Communications in Heat and Mass Transfer, 2010. **37**(8): p. 950-957.
- [2] Barrios-Pina, H., S. Viazzo and C. Rey, *A numerical study of laminar and transitional mixed convection flow over a backward-facing step*. Computers & Fluids, 2012. **56**: p. 77-91.
- [3] Kherbeet, A.S., H. Mohammed and B. Salman, *The effect of nanofluids flow on mixed convection heat transfer over microscale backward-facing step*. International Journal of Heat and Mass Transfer, 2012. **55**(21-22): p. 5870-5881.
- [4] Lan, H., B. Armaly and J. Drallmeier, *Three-dimensional simulation of turbulent forced convection in a duct with backward-facing step*. International Journal of Heat and Mass Transfer, 2009. **52**(7-8): p. 1690-1700.
- [5] Cheng, J.-C. and Y.-L. Tsay, *Effects of solid and slotted baffles on the convection characteristics of backward-facing step flow in a channel*. Heat and mass transfer, 2006. **42**(9): p. 843-852.
- [6] Fathinia, F., A. Heshmati, M. Parsazadeh, M.A. Wahid and M.M. Sies. *The Influence of Various Inlet Geometries on Mixed Convection Flow of Ethylene Glycol in a Backward Facing Step*. in *Applied Mechanics and Materials*. 2013. Trans Tech Publ.
- [7] Kumar, A. and A.K. Dhiman, *Effect of a circular cylinder on separated forced convection at a backward-facing step*. International Journal of Thermal Sciences, 2012. **52**: p. 176-185.
- [8] Nie, J.H., Y. Chen and H.-T. Hsieh, *Effects of a baffle on separated convection flow adjacent to backward-facing step*. International Journal of Thermal Sciences, 2009. **48**(3): p. 618-625.
- [9] Barton, I., *Laminar flow over a backward-facing step with a stream of hot particles*. International Journal of Heat and Fluid Flow, 1997. **18**(4): p. 400-410.
- [10] Rouizi, Y., M. Girault, Y. Favennec and D. Petit, *Model reduction by the Modal Identification Method in forced convection: Application to a heated flow over a backward-facing step*. International Journal of Thermal Sciences, 2010. **49**(8): p. 1354-1368.
- [11] Shih, C. and C.-M. Ho, *Three-dimensional recirculation flow in a backward facing step*. Journal of fluids engineering, 1994. **116**(2): p. 228-232.
- [12] Chiang, T., T.W. Sheu and S. Tsai, *Topological flow structures in backward-facing step channels*. Computers & fluids, 1997. **26**(4): p. 321-337.
- [13] Chiang, T. and T.W. Sheu, *Vortical flow over a 3-D backward-facing step*. Numerical Heat Transfer, Part A Applications, 1997. **31**(2): p. 167-192.
- [14] Nie, J. and B.F. Armaly, *Three-dimensional convective flow adjacent to backward-facing step-effects of step height*. International journal of heat and mass transfer, 2002. **45**(12): p. 2431-2438.
- [15] Armaly, B., A. Li and J. Nie, *Three-dimensional forced convection flow adjacent to backward-facing step*. Journal of thermophysics and heat transfer, 2002. **16**(2): p. 222-227.
- [16] Saldana, J.B., N. Anand and V. Sarin, *Forced convection over a three-dimensional horizontal backward facing step*. International Journal for Computational Methods in Engineering Science and Mechanics, 2005. **6**(4): p. 225-234.
- [17] Heshmati, A., H.A. Mohammed, M. Parsazadeh, F. Fathinia, M.A. Wahid, M.M. Sies and A. Saat. *Effect of vertical baffle installation on forced convective heat transfer in channel having a backward facing step*. in *Applied Mechanics and Materials*. 2013. Trans Tech Publ.
- [18] Mohammed, H., A. Al-aswadi, H. Abu-Mulaweh and N. Shuaib, *Influence of nanofluids on mixed convective heat transfer over a horizontal backward-facing step*. Heat Transfer—Asian Research, 2011. **40**(4): p. 287-307.

- [19] Mohammed, H., A. Al-Aswadi, M. Yusoff and R. Saidur, *Buoyancy-assisted mixed convective flow over backward-facing step in a vertical duct using nanofluids*. Thermophysics and Aeromechanics, 2012. **19**(1): p. 33-52.
- [20] Mohammed, H., A. Al-Aswadi, H. Abu-Mulaweh, A.K. Hussein and P.R. Kanna, *Mixed convection over a backward-facing step in a vertical duct using nanofluids—buoyancy opposing case*. Journal of Computational and Theoretical Nanoscience, 2014. **11**(3): p. 860-872.
- [21] Mohammed, H., A. Al-Aswadi, N. Shuaib and R. Saidur, *Convective heat transfer and fluid flow study over a step using nanofluids: a review*. Renewable and Sustainable Energy Reviews, 2011. **15**(6): p. 2921-2939.
- [22] Murshed, S., K. Leong and C. Yang, *Enhanced thermal conductivity of TiO₂—water based nanofluids*. International Journal of thermal sciences, 2005. **44**(4): p. 367-373.
- [23] Timofeeva, E.V., A.N. Gavrilov, J.M. McCloskey, Y.V. Tolmachev, S. Sprunt, L.M. Lopatina and J.V. Selinger, *Thermal conductivity and particle agglomeration in alumina nanofluids: experiment and theory*. Physical Review E, 2007. **76**(6): p. 061203.
- [24] Zhang, X., H. Gu and M. Fujii, *Effective thermal conductivity and thermal diffusivity of nanofluids containing spherical and cylindrical nanoparticles*. Experimental Thermal and Fluid Science, 2007. **31**(6): p. 593-599.
- [25] He, Y., Y. Jin, H. Chen, Y. Ding, D. Cang and H. Lu, *Heat transfer and flow behaviour of aqueous suspensions of TiO₂ nanoparticles (nanofluids) flowing upward through a vertical pipe*. International journal of heat and mass transfer, 2007. **50**(11-12): p. 2272-2281.
- [26] Abu-Nada, E., *Application of nanofluids for heat transfer enhancement of separated flows encountered in a backward facing step*. International Journal of Heat and Fluid Flow, 2008. **29**(1): p. 242-249.
- [27] Corcione, M., *Heat transfer features of buoyancy-driven nanofluids inside rectangular enclosures differentially heated at the sidewalls*. International Journal of Thermal Sciences, 2010. **49**(9): p. 1536-1546.
- [28] Ghasemi, B. and S. Aminossadati, *Brownian motion of nanoparticles in a triangular enclosure with natural convection*. International Journal of Thermal Sciences, 2010. **49**(6): p. 931-940.
- [29] Vajjha, R.S. and D.K. Das, *Experimental determination of thermal conductivity of three nanofluids and development of new correlations*. International Journal of Heat and Mass Transfer, 2009. **52**(21-22): p. 4675-4682.
- [30] Vajjha, R.S., D.K. Das and D.P. Kulkarni, *Development of new correlations for convective heat transfer and friction factor in turbulent regime for nanofluids*. International Journal of Heat and Mass Transfer, 2010. **53**(21-22): p. 4607-4618.